Received: 17 August 2019 | Revised: 1 October 2019 | Accepted: 2 October 2019

DOI: 10.1002/aoc.5327

FULL PAPER

Applied Organometallic Chemistry WILEY

Oxidovanadium (IV) and iron (III) complexes with O_2N_2 donor linkage as plausible antidiabetic candidates: Synthesis, structural characterizations, glucose uptake and model biological media studies

Manasa Kongot[1] | Dinesh S. Reddy[1] | Vishal Singh[2] | Rajan Patel[3] | Nitin Kumar Singhal[2] | Amit Kumar[1]

[1]Centre for Nano and Material Sciences, Jain University, Jain Global Campus, Bengaluru, 562112, Karnataka India

[2]National Agri Food Biotechnology Institute, Mohali, 140306, India

[3]Biophysical Chemistry Laboratory, Centre for Interdisciplinary Research in Basic Sciences, Jamia Millia Islamia (A Central University), New Delhi, 110025, India

Correspondence
Amit Kumar, Centre for Nano and Material Sciences, Jain University, Jain Global Campus, Bengaluru, 562112, Karnataka, India.
Email: amit.kumar@jainuniversity.ac.in

Funding information
Nano Mission Council, Department of Science and Technology, Grant/Award Number: SR/NM/NS-20/2014; Science and Engineering Research Board, Grant/Award Number: SB/FT/CS-100/2013; Nanomission project, Grant/Award Number: SR/NM/NS-20/2014; Department of Science and Technology (DST), Grant/Award Number: BT/PR10353/PFN/20/889/2013; Science and Engineering Research Board (SERB), India, Grant/Award Number: 100/2013

With the upsurging cases of type II diabetic patients, the demand for safe and effective oral antidiabetic drugs is also increasing. Coordination complexes have proven their mettle as efficient oral drug candidates, which thereby motivated us in this work to design new transition metal complexes as plausible candidates for the treatment of diabetes. A reduced salen ligand, $\{H_2(hpdbal)_2$-an$\}$ (**1**) derived vanadium (IV) and iron (III) complexes, namely, $[V^{IV}O\{(hpdbal)_2$-an$\}]$ (**2**) and $[\{Fe^{III}(OH_2)((hpdbal)_2$-an$)\}_2\ \mu_2$-$SO_4]$ (**3**) were synthesized in this study. The newly obtained ligand and complexes were characterized using usual analytical and spectroscopic techniques. The potential of these compounds in inducing increased glucose uptake by diabetic cells were studied by using insulin resistant HepG2 cells as model diabetic cells and 2-NBDG molecule as a D-glucose analogue and fluorescent tracker. The cells added with the vanadium (IV) complex **3** induced significant NBDG uptake of 95.4% which was higher than that induced by metformin, the standard antidiabetic drug. To elucidate the behavior of the complexes in biological media, model solution studies were conducted with a wide range of pH conditions and protein bovine serum albumin (BSA). The complexes demonstrated effective binding with BSA which was concluded through spectroscopic titration studies and were also found to be sufficiently stable over physiological pH conditions. The study can thus prove to be beneficial in the quest for new antidiabetic drugs.

KEYWORDS

antidiabetic, BSA interaction, O_2N_2 donor ligand, oxovanadium (IV) complex, sulphate bridged iron (III) complex

1 | INTRODUCTION

Diabetes mellitus or more commonly known as 'sugar' is a chronic metabolic disorder characterized by high levels of blood glucose. This is a serious and globally prevailing condition which leads to organ damage, dysfunction and failure.1a In 2014, 422 million adults all over the world were living with diabetes. The global prevalence has doubled from 4.7% in 1980 to 8.5% in 2014. According to the recent statistics reported by the International Diabetes

Federation for the year 2017, the number has raised to 425 million people and it is expected that by 2045, this disease will take a toll on 629 million people.1b Type 2 diabetes also termed previously as adult-onset or non-insulin dependent diabetes is the most serious and prevailing type and in the recent days, majority of people suffer with this type of diabetes owing to depleting standards of lifestyle. Many successful approaches for the treatment of elevated blood glucose levels have been accomplished due to extensive research and development studies. Several classes of oral drugs[2] such as sulfonylureas, biguanides, glucosidase inhibitors, DPP-4 inhibitors and SGLT2 inhibitors have been established in the past few decades which have been able to help the body to control blood glucose levels. Although these classes of drugs have been successful, they pose many adverse side effects such as abdominal and gastrointestinal discomforts, diarrhoea, drug intolerance, hypoglycaemia, weight gain, hepatotoxicity, bone density reduction and fracture risks, nausea, cardiovascular disease risks and genital infections.[3–7]- Medicinal inorganic chemistry is one of the hopes for overcoming the glitches posed by existing organic drugs,[8] speaking of which, trace metals such as vanadium and iron have huge scope and have been studied for their biological and therapeutic activities. Vanadium constitutes 0.015% of earth's crust and is well distributed in nature.[9,10] Several ascidian sea squirts and amanita mushrooms are known to accumulate vanadium in the form of vanadate (vanadium(V)oxoanion) and amavadin (non-oxovanadium (IV) complex) respectively.[11,12] Vanadium containing enzymes such as vanadium bromoperoxidases occur in many marine algae, fungi, eukaryotes and they function as a catalyst for the formation of most of the naturally available brominated compounds.[13] Citing these biological significances of vanadium, researchers have developed many nature-mimicking and synthetic vanadium compounds for exploration of their biological activities mainly towards therapeutic usages. More than a century ago, a vanadium compound, sodium vanadate was used as a medicinal agent for the treatment of elevated blood glucose levels in body.[14] After nearly a century leap, in 1985, Heyliger and his group's first report[15] on the blood glucose lowering effect of sodium vanadate in streptozotocin (STZ)-induced diabetic rats generated high scientific inquisitiveness amongst researchers about the use of vanadium compounds in treatment of diabetes. This curiosity led to the development of bis (maltolato)oxovanadium (IV) (BMOV) and its analogue bis (ethylmaltolato) oxovanadium (IV) (BEOV) which have proved their suitability as insulin enhancing agents with improved bioavailability and have successfully undergone pre-clinical testing for efficacy and safety.[16,17] The latter has effectively completed phase I clinical trials and is under study in the phase II trials for treatment of type II diabetes patients.[18] A vanadium picolinato complex, [VO_2dipic$^-$] is another potent antidiabetic agent which has helped in curing cats affected with diabetes.[19] The pyridine oxothiolato based complex, [VO (opt)$_2$] and acetylacetone based complex, [VO (acac)$_2$] have exhibited robust insulin mimetic activity by normalizing blood glucose levels in STZ-rats upon oral administration.[20,21] Numerous oxidovanadium (I*V*/V) complexes derived from salen and salan type of ligands have exhibited excellent *in vitro* and *in vivo* insulin enhancing activity by lowering blood glucose levels in STZ induced-rats. $V^{IV}O$ (salen) can reverse hyperglycemia to normal glucose levels in alloxan-induced diabetic rats.[22] Another trace metal iron is the fourth most common element constituting about 5% of the Earth's crust.[23] Iron is required for smooth and normal functioning of many biological processes.[24] In humans, haemoglobin, cyctochrome and catalase are three important biomolecules consisting of iron in them.[25] These iron containing proteins are responsible for transport, storage and use of oxygen, electron transfer and biocatalysis reactions. One of the very first reports of therapeutic uses of iron was that of ferrocenium salts which exhibited exceptional anticancer activities.[26,27] Following this, many iron complexes have been reported for their exceptional anticancer and antibacterial activities.[28,29] Especially, salen tethered iron (III) complexes have shown detrimental effects on cancer cells whose activities were higher than cisplatin drug.[30,31] However, there have been no significant reports on the antidiabetic potential of iron complexes.

To address the impending type II diabetes disease burden, in the present study, new oxidovanadium (IV) and iron (III) complexes affixed with a 'salan' type of ligand have been prepared (Scheme 1). The moieties were preliminarily screened for their antidiabetic activity through glucose uptake studies on model diabetic cells (insulin resistant HepG2 cells). The response of these compounds in biological media was stipulated by studying their behavior in varied pH conditions and protein (BSA) solution.

2 | EXPERIMENTAL METHODS

2.1 | Materials and instrumentation used

For all the experiments, solvents and chemicals used were of synthesis grade and were used as received. Vanadyl acetylacetonate, [VO (acac)$_2$] was prepared by following a very well-known procedure[32] using

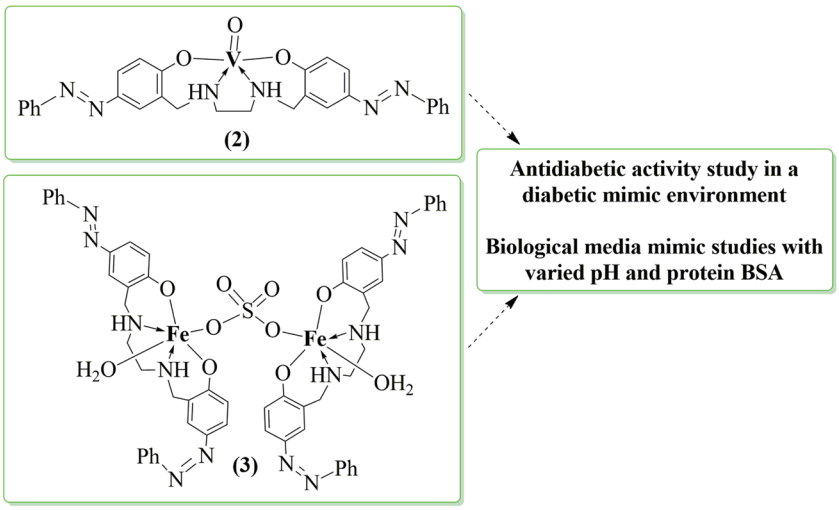

SCHEME 1 Representation of the complexes obtained in this study and the biological activity studies performed for them

vanadium pentoxide (V_2O_5) and acetyl acetone. Ferrous sulphate heptahydrate (purity >98%) was obtained from S D Fine-Chem Ltd., India. Bovine serum albumin (BSA, purity >99%, fraction V, fatty acid free, lyophilized powder) was purchased from Sisco Research Laboratories Pvt. Ltd., India. 2-hydroxy-5-(phenyldiazenyl)benzaldehyde (Hhpdbal) was prepared by following the method used in our previously published work.[33] The synthetic protocols followed for obtaining the reduced imine ligand system and their respective vanadium and iron complexes are outlined in detail in Section 3.4.

Elemental analysis was done using a CHN elemental analyzer, Euro Vector E-3000 and energy dispersive X-ray analyzer, JEOL-JSM7100F. Infrared spectra were measured using a Bruker Alpha Single reflection ATR setup equipped with ZnSe crystal. Electronic spectra were measured using a UV–Vis spectrophotometer, Shimadzu UV-1800. NMR spectra, ^{1}H-NMR and ^{13}C-NMR were recorded for the ligand using an Agilent 400MR DD2 FT-NMR Spectrometer and tetramethylsilane as internal standard. Electron paramagnetic resonance spectra, X-band, were obtained from a ESR Spectrometer, JEOL JES-FA200 at 77.2 K. Thermal analysis of the complexes was performed on a TG/DTA analyzer, Perkin Elmer STA 6000 up to 700 °C.

2.2 | Antidiabetic/glucose-uptake studies

The glucose uptake activity induced by the complexes was evaluated with the help of 2-NBDG assay. This assay was performed by following previously established protocol.[34] The model cells used for this study were human liver carcinoma cells, HepG2 which were induced with insulin resistivity to mimic diabetic environment. For this, the cells were grown in a 96-well plate up to 90% confluency and then treated with insulin resistance inducing mixture of tumor necrosis factor (TNF-α), fructose and palmitic acid. These cells were then added with different concentrations of the test complexes **2** and **3**. The cells added with well-known antidiabetic drug metformin and ligand **1** were taken as standard and reference respectively for the experiments. HepG2 cells which were not added with any insulin resistance media and study compounds were taken as control for the experiments. The cells which were induced with insulin resistivity were taken as the test for the experiments. All the cells were incubated for 24 hr and thereafter the wells were washed with buffer PBS (1X). In succession, the fluorescent analogue of D-glucose, 2-NBDG (40 μM) and insulin (0.1 μM) were added and incubated for an hour. The wells were then carefully washed with PBS and lysis buffer was added. The fluorescence given out from each well were carefully measured using a fluorescence spectrophotometer.

2.3 | Protocol for model biological media studies

Varied pH experiments were conducted on the solution of the synthesized complexes and for this, pH meter calibrated with standard buffers and UV–Vis spectrometer were used. The mode of interaction of the compounds with a serum protein, bovine serum albumin (BSA) was studied using steady-state, synchronous, three-dimensional fluorescence spectroscopy techniques, temperature probed UV–Visible spectroscopy and infrared spectroscopy techniques. The instruments used were a Varian Cary Eclipse spectrofluorometer, Analytik Jena Specord-250 spectrophotometer and Specac golden gate ATR instrument. The stock solutions of BSA (5 μM) and

complexes **2**, **3** (1 mM each) were prepared in sodium phosphate buffer of pH 7.4 and DMSO respectively.

2.4 | Synthesis

2.4.1 | Synthesis of O_2N_2 donor ligand, 2,2′-((ethane-1,2-diylbis (azanediyl))bis (methylene)) bis (4-(phenyldiazenyl) phenol) {H_2(hpdbal)$_2$-an} (1)

To a solution of 2-hydroxy-5-(phenyldiazenyl)benzaldehyde (2.26 g, 10 mM) in 20 ml of dichloromethane, added ethylene diamine (0.33 ml/0.30 g, 5 mM) slowly. This reaction mixture was kept for stirring at room temperature for 4 hr (Scheme 2). Golden yellow colored precipitate was obtained which was isolated after filtration under vacuum. Subsequently, it was washed with dichloromethane, diethyl ether and left for drying in a hot air oven at 60 °C to obtain the product **A**.

A solution of the imine compound, {H_2(hpdbal)$_2$-en} (**A**) (2.38 g, 5 mM) in 15 mL of methanol and dichloromethane mixture was maintained at 0 °C. To this solution, a methanolic solution of sodium borohydride (0.45 g, 12 mM) containing few drops of conc. KOH solution was slowly added with stirring (Scheme 2). The pH was set to 6 by adding required amount of HCl and the reaction mixture was stirred for about 6–7 hr. TLC monitoring confirmed gradual decrease in the imine content and gradual increase in the amine content following reduction. As soon as the TLC spot for the imine compound disappeared, the solvent in the reaction mixture was evaporated to dryness and about 10 ml of water was added to the residue followed by pH maintenance of 4–5. The obtained yellow product was vacuum filtered, washed with distilled water, diethyl ether and left for drying in a hot air oven at 50 °C to obtain the new ligand, **1**.

{H_2(hpdbal)$_2$-en} (A): Yield: 3.90 g, 82%; Anal. calcd. For. $C_{28}H_{24}N_6O_2$ (MW: 476.53 g mol^{-1}): C, 70.57; H, 5.08; N, 17.64. Found: C, 70.43; H, 5.01; N, 17.59; Selected ATR-IR data (ν/cm^{-1}): 1630 (C=N), 1592, 1484 (N=N), 1286 (C-N), 3053 (aromatic C-H), 1231 (C-O); ^{1}H-NMR (400 MHz, $CDCl_3$): δ 13.75 (s, 2H, aromatic O-H), 8.50 (s, 2H, N=C-H), 7.98–7.05 (m, 16H, aromatic H), 4.03 (s, 4H, -CH_2-CH_2); ^{13}C-NMR (400 MHz, $CDCl_3$): δ 59.37 (2C), 118.04 (2C), 122.51 (6C), 126.95 (2C), 127.35 (2C), 128.99 (4C), 130.39 (2C), 145.33 (2C), 152.64 (2C), 164.23 (2C), 166.37 (2C).

{H_2(hpdbal)$_2$-an} (1): Yield: 1.87 g, 78%; m.p: 238 °C; Anal. calcd. For. $C_{28}H_{28}N_6O_2$ (MW: 480.56 g mol^{-1}): C, 69.98; H, 5.87; N, 17.49. Found: C, 69.96; H, 5.84; N, 17.52; Selected ATR-IR data (ν/cm^{-1}): 1598, 1444 (N=N), 1285 (C-N), 3023 (aromatic C-H), 2757 (aliphatic C-H), 1158 (C-O), 3376 (N-H); ^{1}H-NMR (400 MHz, DMSO-d_6): δ 8.04 (s, 2H, aromatic O-H), 7.85–7.19 (m, 16H, aromatic H), 4.20 (s, 4H, Ar-CH_2-N), 3.37 (s, 4H,-CH_2-N); ^{13}C-NMR (400 MHz, DMSO-d_6): δ 43.58 (2C), 45.79 (2C), 116.49 (2C), 119.68 (2C), 122.55 (4C), 125.84 (2C), 126.94 (2C), 129.85 (4C), 131.16 (2C), 145.29 (2C), 152.49 (2C), 160.00 (2C).

2.4.2 | Synthesis of vanadium (IV) complex, [$V^{IV}O${(hpdbal)$_2$-an}] (2)

Vanadyl acetylacetonate, [$V^{IV}O$ (acac)$_2$] (0.56 g, 2.1 mM) was taken in 20 ml of methanol and to this was added a solution of ligand, {H_2(hpdbal)$_2$-an} (**1**) (0.96 g, 2.0 mM) dissolved in 20 ml of methanol. The reaction mixture was refluxed for 3 hr with stirring (Scheme 3). The initial light brown colored solution turned into dark brown and this solution was reduced to half of its volume after reflux. The solution was then filtered to get a clear dark brown solution. This filtrate upon room temperature evaporation gave dark brown colored precipitate of **2** which was separated, washed with diethyl ether and dried in anhydrous conditions. Yield: 0.83 g, 76%; m.p: 278 °C; Anal. calcd. For. $C_{28}H_{26}N_6O_3V$(MW: 545.49 g mol^{-1}): C, 61.65; H, 4.80; N, 15.41. Found: C, 61.62; H, 4.82; N, 15.38; Selected ATR-IR data (ν/cm^{-1}): 3418 (N-H), 1470, 1579 (N=N), 1108 (C-O), 1358 (C–N), 3066–3037 (aromatic C-H), 2934–2872 (aliphatic C–H), 982 (V=O); UV–Vis (λ_{max}/nm): 347, 448, 612.

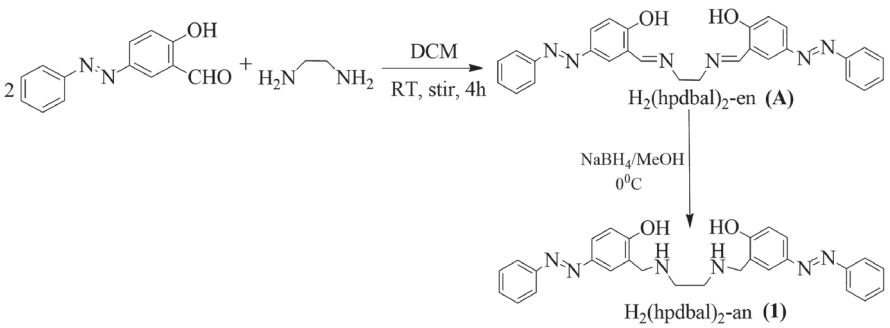

SCHEME 2 Synthetic route to obtain the ligand used in the present study, {H_2(hpdbal)$_2$-an} (**1**)

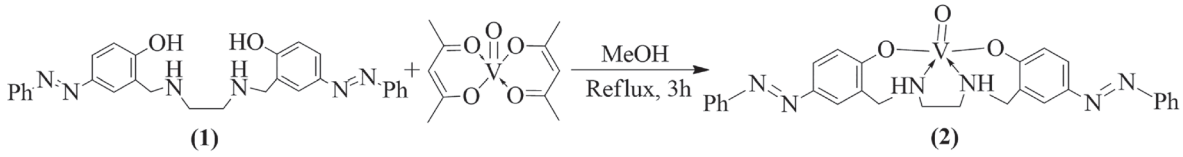

SCHEME 3 Synthetic route to obtain [$V^{IV}O${(hpdbal)$_2$-an}] (**2**)

2.4.3 | Synthesis of iron (III) complex, [{Fe^{III} (OH_2)((hpdbal)$_2$-an)}$_2$ μ_2-SO_4] (3)

The ligand, {H_2(hpdbal)$_2$-an} (**1**) (0.96 g, 2.0 mM) was dissolved in 20 ml methanol and to this, methanolic ferrous sulphate heptahydrate (0.58 g, 2.1 mM) solution was added. The reaction mixture immediately turned to dark brown color and this mixture was refluxed for 1 hr to obtain a dark brown colred precipitate of complex **3** (Scheme 4). The hot solution was filtered to separate out the residue which was then washed with methanol and diethyl ether. The product obtained was then dried in an hot air oven at 70 °C. Yield: 1.86 g, 78%; m.p: 232 °C; Anal. calcd. For. $C_{56}H_{56}N_{12}O_{10}SFe_2$ (MW: 1200.87 g mol^{-1}): C, 56.01; H, 4.70; N, 14.00. Found: C, 55.94; H, 4.71; N, 14.09; Selected ATR-IR data (ν/cm^{-1}): 1068 (S=O), 1391 (SO_4), 1480, 1556 (N=N), 1103 (C-O), 1305 (C–N), 3003 (aromatic C–H), 2883–2996 (aliphatic C-H), 3332 (O-H), 1639, 3242 (N-H); UV–Vis (λ_{max}/nm): 347, 461, 624.

3 | RESULTS AND DISCUSSION

3.1 | Characterization

The elemental analysis of the newly obtained ligand and complexes were done with the help of CHN and EDS analysis. The data obtained for the basic elemental composition of the compounds were found to be in agreement with the calculated values. The presence of metals, vanadium and iron was confirmed in compounds **2** and **3** respectively (Figure 1).

The important functional groups present in the compounds were confirmed by the characteristic IR spectra (Figure 2). The ligand H_2(hpdbal)$_2$-an (**1**) exhibited a typically broad phenolic O-H stretching vibrational peak and secondary amine N-H stretching at 3307 and 3376 cm^{-1} respectively. The corresponding vanadium complex, [$V^{IV}O${(hpdbal)$_2$-an}] (**2**) did not show any peak

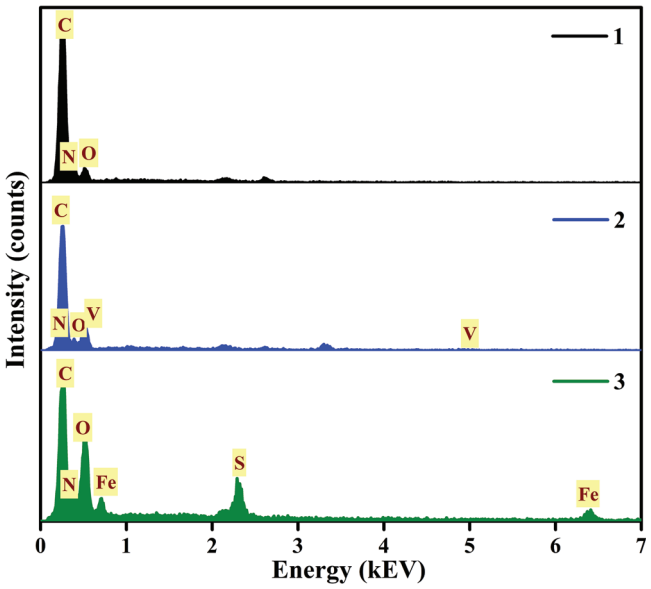

FIGURE 1 Representative EDS analysis which confirms the elemental composition of the ligand (**1**) and complexes (**2** and **3**)

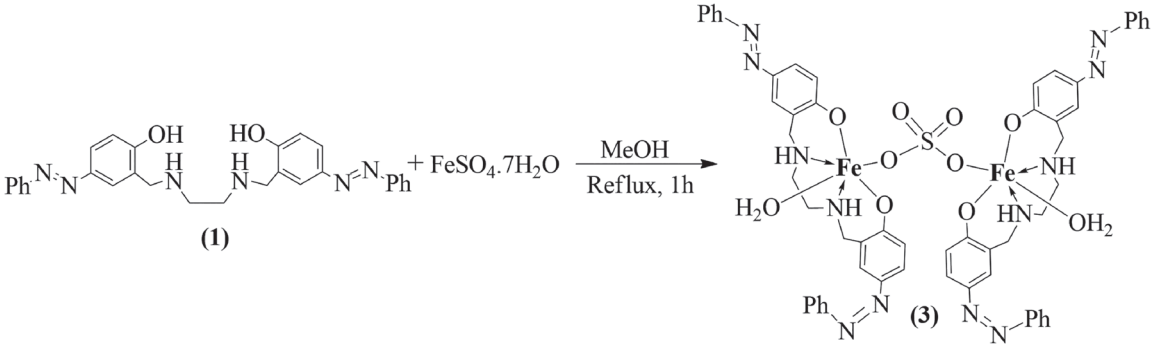

SCHEME 4 Synthetic route to obtain [{Fe^{III} (OH_2)((hpdbal)$_2$-an)}$_2$ μ_2-SO_4] (**3**)

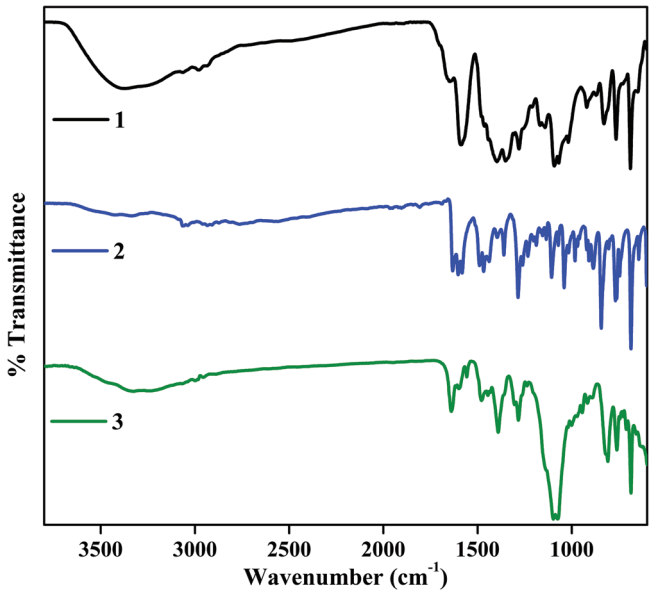

FIGURE 2 Vibrational spectra representing the stretching and bending modes of functional groups present in the ligand and complexes

for O-H stretching which confirms the participation of phenolate O in bonding to vanadium center by losing its proton. In addition, a signal for the vanadium-oxo bond stretching was observed at 982 cm^{-1}. No significant changes were observed for other vibrational bands and all peaks pertaining to other parts of the ligand appeared within the anticipated range. In the IR spectra of iron complex, [{Fe^{III} (OH_2)((hpdbal)$_2$-an)}$_2$ μ-O_2SO_2] (**3**), shifts were observed for C-O and N-H stretching corresponding to the phenolato oxygen and amine nitrogen which coordinates to the metal center. O-H stretching bands were observed corresponding to the coordinated water molecules. Notably, a strong band for S=O stretching at 1068 cm^{-1} and peak particular to the SO_4 group at 1391 cm^{-1} were observed. This accounts for the sulphate bridged (μ_2-SO_4) coordination with two iron metal centers. All other stretching and bending vibrations of the complex stayed intact which confirms the complexation by the ligand.

The excitation properties of the compounds were studied by their electronic spectra recorded in DMSO (SI Figure 1). The UV–Vis spectrum of the ligand **1** displayed a peak at 347 nm which can be related to the absorption of energy for the intra-ligand n-π* transition. The complexes exhibited charge transfer shoulder bands in the range of 448–461 nm. A low energy band corresponding to the forbidden d-d transition was observed in the range of 612–624 nm for both vanadium and iron complexes. The intra ligand peaks were retained with slight shifts in the complexes.

The X-band EPR spectra of the vanadium (IV) complex **2** and iron (III) complex **3** were recorded in DMSO solution (5×10^{-4} M) at 77 K owing to the paramagnetic nature of the V (IV) and Fe (III) species. Since the nuclear spin of V^{+4} is 7/2, a typical EPR spectrum of a vanadium (IV) complex should consist of 8 hyperfine splitting lines and this was evident from the EPR spectrum obtained for the complex **2** (Figure 3). This spectrum was simulated manually to calculate the spin-Hamiltonian parameters which are given in table 1. The compound exhibited an axial spectrum with $g_x = g_y = g_⊥ > g_z = g_{||}$. The hyperfine splitting constant ($A_z = A_{||}$) value obtained from the spectrum was correlated with the number and type of ligand environment equatorially present around the vanadyl ion using the "additivity" rule proposed by Holyk and Chasteen.[35]

The obtained $A_{||}$ value of 157.7 x 10^{-4} cm^{-1} matched very well with the theoretically obtained value for $A_{||}$ using the additivity rule. The value corresponds to two N_{amine}, N_{amine} and two O_{ArO-}, O_{ArO-} equatorially placed donor sets which is in accordance with the expected structure of the vanadyl complex **2**. All the spin parameters obtained are characteristic of d_{xy}^1 configuration of the VO^{2+} ion in an axially compressed fashion[36] and the oxovanadium (IV) complex exists in a slightly distorted square pyramidal geometry[37] around the phenolato and amine donor sets. The Fe (III) species with a nuclear spin of $I = 1/2$ gave an anisotropic and complex splitting pattern with the g value centered at 2.03 which suggested an octahedral geometry and low spin Fe (III) metal center.[38]

Distinct weight loss steps could not be identified in the TGA analysis profile of the vanadium complex **2**. The thermal degradation steps involved firstly the loss of

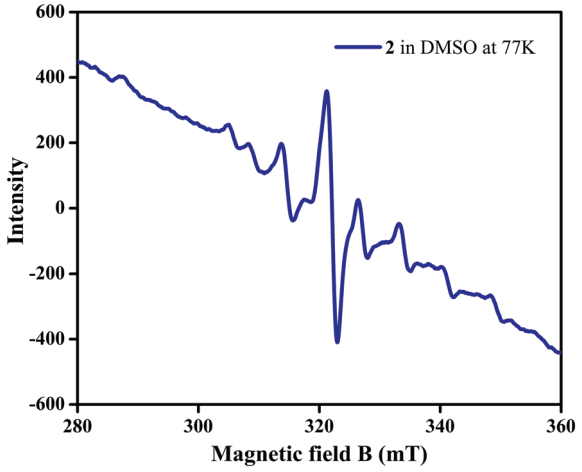

FIGURE 3 Manually simulated EPR spectrum of the vanadium (IV) species (**2**) with the characteristic hyperfine splitting of 8 lines

TABLE 1 Spin-Hamiltonian parameters acquired from the EPR spectrum of $[V^{IV}O\{(hpdbal)_2\text{-an}\}]$ (**2**) in DMSO

Sample	$g_x=g_y=g_\perp$	$g_z=g_\parallel$	g_{iso}	$A_x=A_y=A_\perp$ (10^{-4} cm^{-1})	$A_z=A_\parallel$ (10^{-4} cm^{-1})	A_{iso}	$\Delta g_\parallel/\Delta g_\perp$	Equatorial donor set
2	1.985	1.951	1.974	59.9	157.7	92.5	2.96	N_{amine}, N_{amine}, O_{ArO-}, O_{ArO-}

amine part of the ligand system between 190-320 °C followed by the loss of whole of organic ligand backbone left in between 320-700 °C. The residual corresponds to the vanadium oxide material which is the end product of the thermal decomposition of compound **2**. The TGA analysis of the binuclear sulphate bridged iron complex **3** (SI Figure 2) showed weight loss characteristic to the predicted structure with the stepwise loss of coordinated water molecules, amine part of the ligand and the whole of ligand backbone in successions with the liberation of sulphur dioxide gas (Scheme 5).

3.2 | Glucose uptake activity studies

The vanadium complex $[V^{IV}O\{(hpdbal)_2\text{-an}\}]$ (**2**) and iron complex $[\{Fe^{III}(OH_2)((hpdbal)_2\text{-an})\}_2\ \mu_2\text{-}SO_4]$ (**3**) were evaluated for their glucose intake inducing abilities by keeping the ligand $\{H_2(hpdbal)_2\text{-an}\}$ (**1**) and standard antidiabetic drug metformin as references. HepG2 cells which were induced with insulin resistance have been used as diabetic model for the study. With the addition of insulin and 2-NBDG, the fluorescence reading given by the cells added with different concentrations of the compounds were noted. The readings were compared with the fluorescence readings from control, test, standard, reference and NBDG molecules alone.

The insulin resistant HepG2 cells showed low uptake of NBDG thereby simulating diabetic environment. When these cells were added with the ligand and complexes, the NBDG uptake was higher. Notably, when the vanadium complex, $[V^{IV}O\{(hpdbal)_2\text{-an}\}]$ (**2**) of 0.1 μM and 0.2 μM concentrations was added, it induced excellent NBDG uptake of 80.8% and 95.4% respectively by the insulin resistant cells. This uptake is quantified by the histogram plot given in Figure 4. The increased glucose

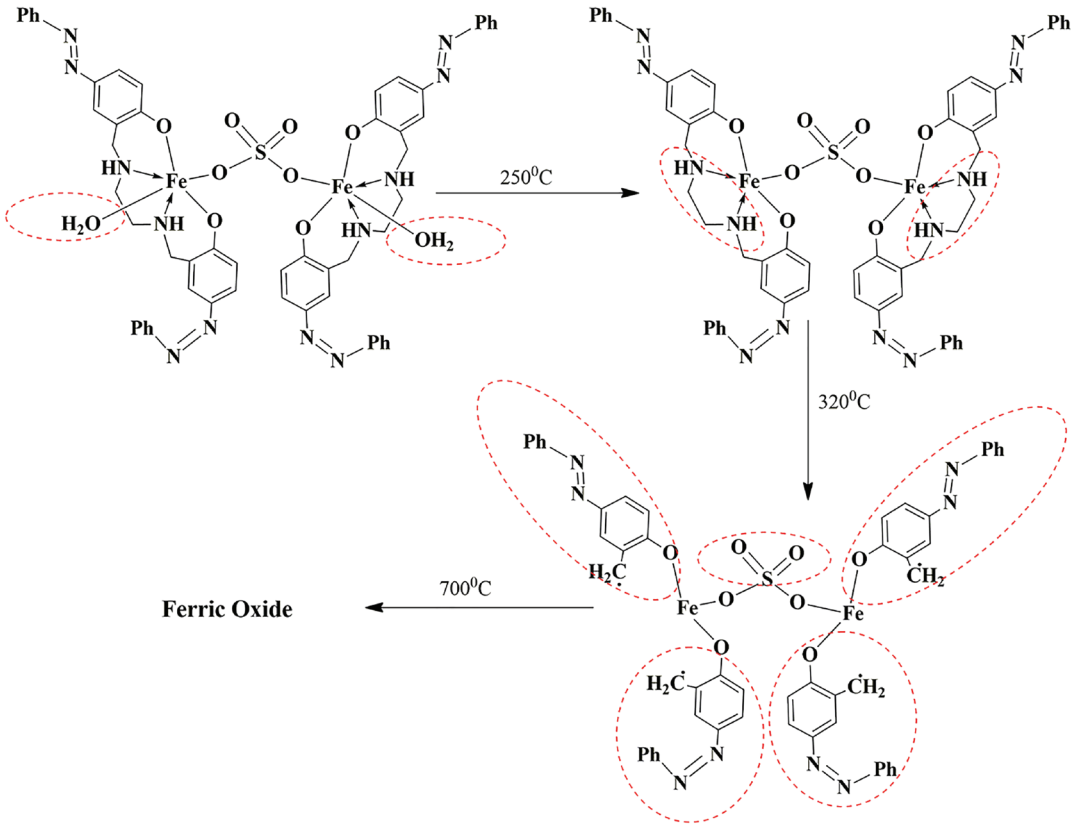

SCHEME 5 Thermal decomposition pathway of the iron (III) species (**3**) as predicted by the TG analysis

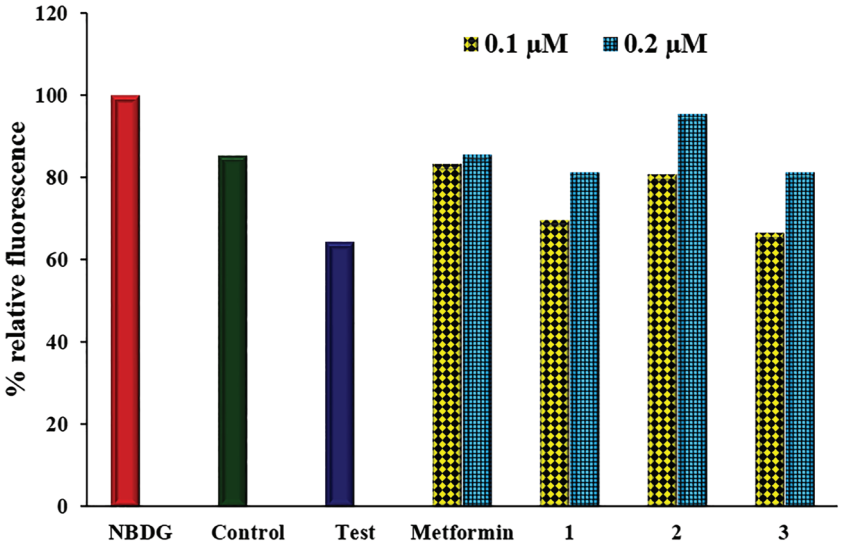

FIGURE 4 Histogram representing the relative fluorescence readings which quantifies the glucose uptake potentials. Here, NBDG is a fluorescent D-glucose analogue used as a tracker, Control is untreated human liver cancer cells (HepG2), Test is the insulin resistant HepG2 cells, Metformin is the standard antidiabetic drug used as reference and **1**, **2** and **3** are the compounds $\{H_2(hpdbal)_2\text{-an}\}$, $[V^{IV}O\{(hpdbal)_2\text{-an}\}]$ and $[\{Fe^{III}(OH_2)((hpdbal)_2\text{-an})\}_2\ \mu_2\text{-}SO_4]$ respectively

uptake potential induced by the V (IV) complex was found to be higher than that induced by the standard antidiabetic drug metformin (85.7% of NBDG uptake at 0.2 μM concentration). Although the Fe (III) complex did not exhibit comparable activity as that of the vanadium complex and standard, it displayed moderate activity which was almost same as that shown by the ligand and standard drug.

3.3 | Biological media simulation studies

To supplement the bioactivity exhibited by the complexes, their behavior in simulated biological media was studied. Firstly, the effect of varied pH conditions (acidic to basic) on the compounds were evaluated with the help of potentiometric pH titrations and UV–Vis spectrophotometric pH titrations. For this study, solutions of complexes **2** and **3** were prepared in water-DMSO mixture (50% (*v*/v)). The initial pH of the solution of compounds was slowly varied in acidic and basic pH ranges of 3–9. From the potentiometric titration readings, the pharmaco-parameter pKa was calculated using the plot of pH vs volume of base added (SI Figure 3). The pKa of both the complexes (pK_a for **2**: 4.98; pK_a for **3**: 4.38) were found to be in the most suitable range of any drug candidate.[39]

From the UV–Vis spectrophotometric titration studies, it was found that the absorption maxima exhibited by the compounds did not shift with varying pH conditions (Figure 5 and SI Figure 4). Absorbance intensity shifts were observed owing to protonation and deprotonation effects on the compounds. The convenient pK_a values and the stability over wide pH range elucidates that both the complexes (**2** and **3**) are bound to be stable in physiological pH conditions prevalent in human serum.

The behavior and interaction modes of the most potent vanadium complex **2** with a model drug carrier protein, BSA were evaluated with the support of emission, absorbance and IR spectra. For the emission and absorbance studies, the spectra were measured for titrations of ten different concentrations of vanadium complex (0 μM to 10 μM) with a fixed concentration of BSA solution (5 μM). The emission spectra were studied using three techniques, viz., steady state, synchronous and three dimensional. In the steady state fluorescence spectra, it was observed that the emission profile of protein at 347 nm due to the amino acid residues got gradually

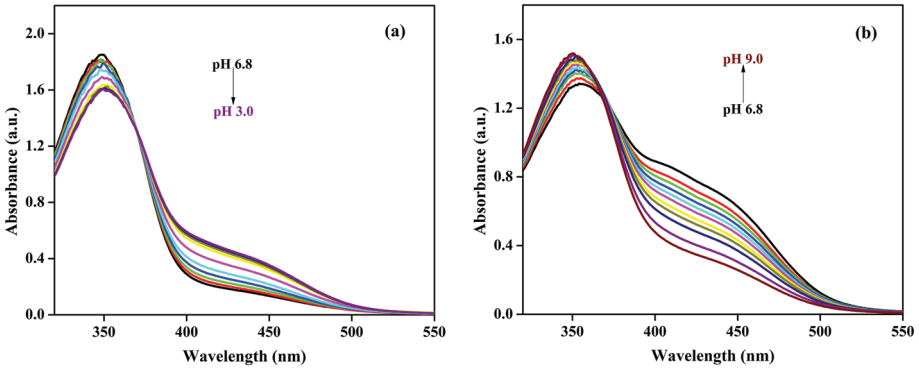

FIGURE 5 UV–Visible spectrophotometric titration studies for $[V^{IV}O\{(hpdbal)_2\text{-an}\}]$ (**2**), the most active antidiabetic compound in **(a)** acidic pH and **(b)** basic pH

quenched with the addition of the compound (SI Figure 5). This quenching pattern was carefully evaluated with the help of Stern-Volmer plot of F_0/F vs C where F_0 and F are the emission intensities of pure BSA and BSA titrated with compound **2** at 347 nm. The graph was observed to be almost linear upon fitting with R^2 value of 0.98 (Figure 6a). This gave a clue on static quenching of the BSA fluorophore. The number of active binding sites (*n*) for the compound to bind with BSA was calculated to be 1.5 using a double log graph (SI Figure 6). For the synchronous fluorescence study, wavelength difference ($\Delta\lambda$) was set at 15 nm and 30 nm for recording the respective fluorescence of tyrosine and tryptophan residues in BSA. It was observed that, with the addition of vanadium complex, the tryptophan emission intensity got quenched to a higher extent than that of the tyrosine residue (Figure 6b).

For the three dimensional fluorescence study, three concentrations (1 μM, 5 μM and 10 μM) of the vanadium complex were titrated with BSA (5 μM) by setting excitation wavelength between 200 nm to 360 nm and emission wavelength between 200 nm to 650 nm. A graph with 3 representative axes *viz.* emission and excitation intensities vs wavelength was obtained from each titration study (Figure 7). These plots gave an evidence of slow unfolding of the coiled secondary structure of protein. In the Figure 7, peak 2 which arises due to the $n \rightarrow \pi^*$ transitions occurring in the protein backbone was found to be quenched by a higher rate than that of the peak 1 which is due to the amino acid residue tryptophan. This observation hence gives a conclusion that the protein secondary structure is prone to be affected with increasing concentrations of the complex, especially above 1:1 molar ratio of complex and protein. For better understanding of this quenching, the quenching percentage after each addition is summarized in a table in the supporting information (SI Table 1).

The absorbance spectra were studied at four different temperatures, *viz.* 20 °C, 25 °C, 30 °C and 35 °C mainly for interpreting the thermodynamics and extent of binding between BSA and the bioactive vanadium compound. At all temperatures, it was observed that the absorbance maxima at 280 nm showed a trend of increment with the addition of increasing concentrations of the complex. The representative spectra at 25 °C is given in Figure 8a. From this study, a double reciprocal plot of $A_0/(A\text{-}A_0)$ vs 1/c was drawn at all temperatures (Figure 8b). The values of binding constants (K_a) obtained were high which concluded a strong binding. In addition, the K_a value was found to decrease with temperature which gives further proof for static quenching of BSA fluorophore. The binding thermodynamic parameters, enthalpy change (ΔH), entropy change (ΔS) and Gibbs' free energy change (ΔG) were calculated from van't Hoff plot ($\ln K_a$ vs 1/T) and Gibbs' free energy relation ($\Delta G = \Delta H\text{-}T\Delta S$). All these parameters were calculated to be of negative values suggesting a spontaneous and exothermic binding reaction occurring between BSA and the compound and that this binding is mostly made of hydrogen bonded and van der Waals interactions.[40]

The absorbance exhibited by the vanadium complex was overlapped with the emission spectrum of pure BSA to get a plot shown in SI Figure 7. From this plot, energy parameters such as efficiency of energy transfer (E), critical distance of proximity needed for efficient binding (R_0) and the vicinity (r) between quencher compound and BSA fluorophore were calculated with the help of FRET equations. All the values obtained were in correlation with the FRET theory associated with non-radiative energy transfer between excited state molecules of protein and ground state quencher molecules.

The vibrational spectra of BSA were studied with the addition of vanadium compound to understand the changes occurring to the amide I band pertaining to the peptide backbone (Figure 9). The amide I band, when deconvoluted, can be seen as a mixture of different secondary structures of the protein with the alpha-helical form being very prominent. With the addition of compound **1**, upon deconvolution of the amide I band region, it was observed that the alpha-helical form was slowly

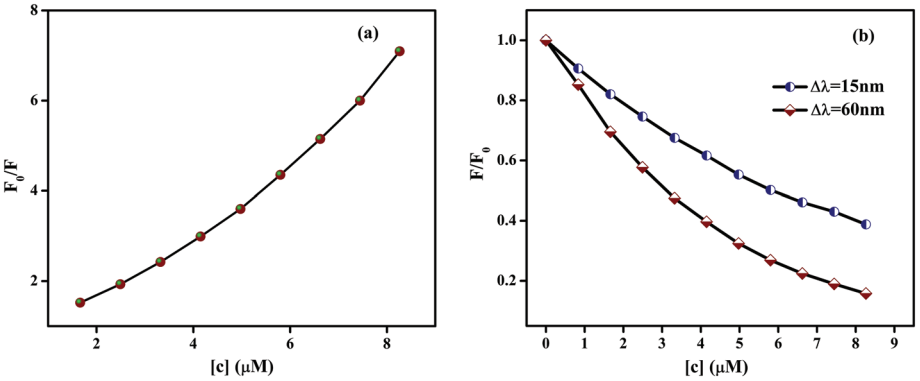

FIGURE 6 Graphs obtained from the emission spectra of BSA titrated with successive concentrations of oxovanadium salan complex. **(a)** Stern-Volmer plot drawn using the steady state fluorescence emission spectra and **(b)** Plot drawn using the synchronous fluorescence spectra measured for tyrosine and tryptophan residues

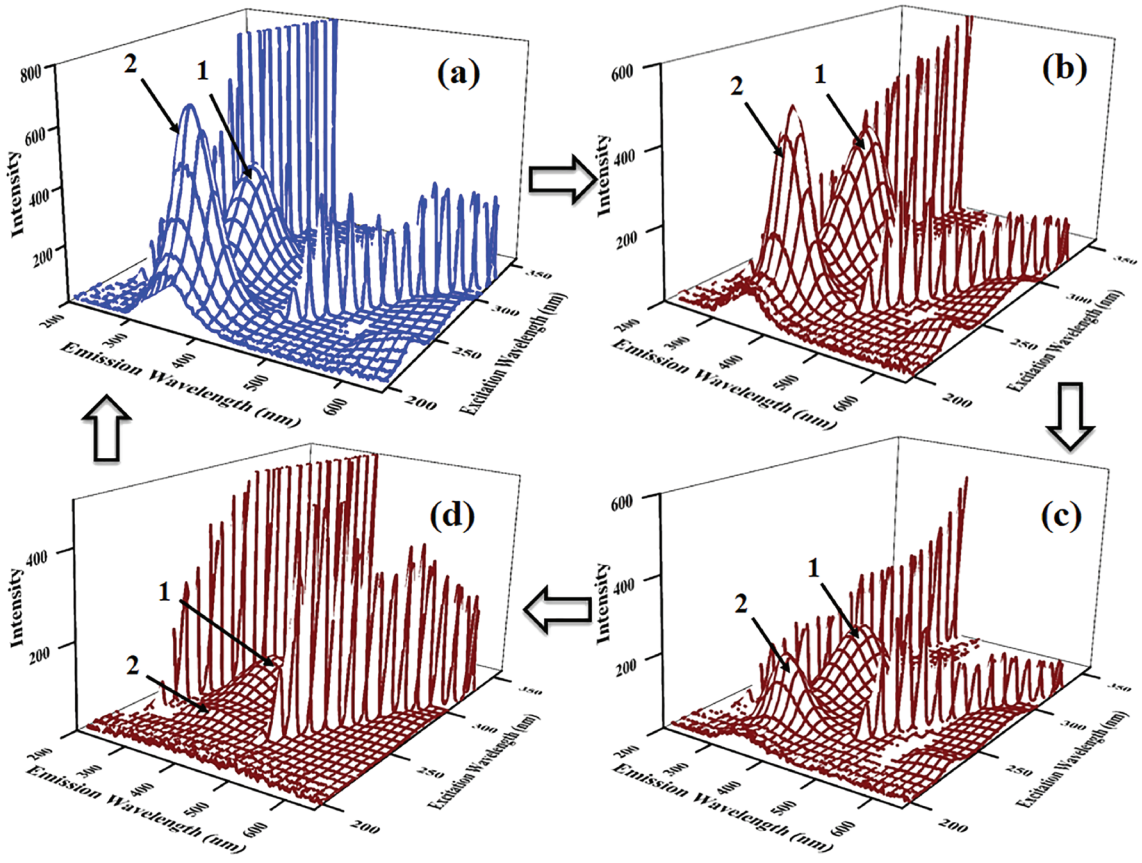

FIGURE 7 Three dimensional fluorescence quenching profile of **(a)** BSA with the addition of increasing concentrations of vanadium complex **(b, c, d)**. Peak 1 represents the fluorescence due to the amino acid tryptophan ($\pi \rightarrow \pi^*$ transitions) and peak 2 represents the fluorescence due to transitions in the protein polypeptide backbone

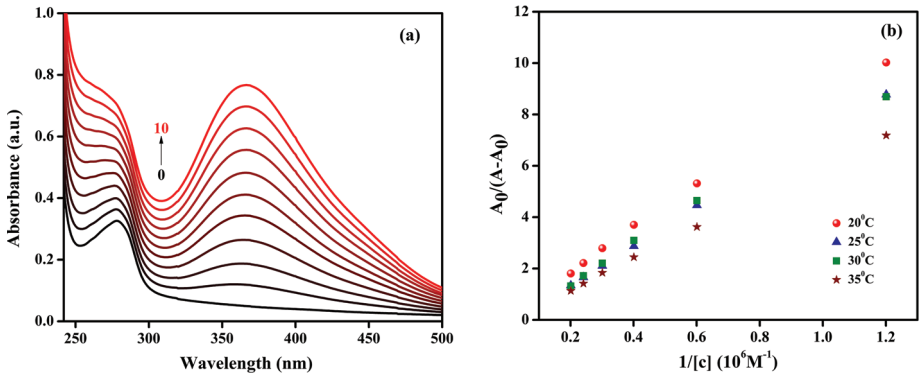

FIGURE 8 **(a)** UV–Vis spectrophotometric spectra of BSA added with different concentrations of vanadium complex. **(b)** Double reciprocal plot for the calculation of binding constant

converting into other secondary forms such as the β-sheets thereby losing its coiled secondary structure and causing denaturation. Although, it is to be noted that this conversion was observed to be prominent at high concentrations of the complex (1:2 ratio of BSA and compound).

The study of interaction of vanadium complex with BSA summarized that the potent drug candidate shows extensive binding and quenching of BSA fluorophore and does not denature the protein structure which thereby concludes that it can bind efficaciously with drug carrier protein.

This study also allows us to predict that the mode of antidiabetic action of the oxovanadium (IV) complex is most likely to be same as that exhibited by most of the potent oxovanadium antidiabetic drug candidates previously developed.[41]The complex is expected to undergo speciation in the first hand in biological media and bind to serum carrier protein such as human serum transferrin. This will then make it way through the biological membrane to bind with the cysteine residue of protein tyrosine phosphatase enzyme, the free end of which is responsible for de-phosphorylation of the insulin receptor

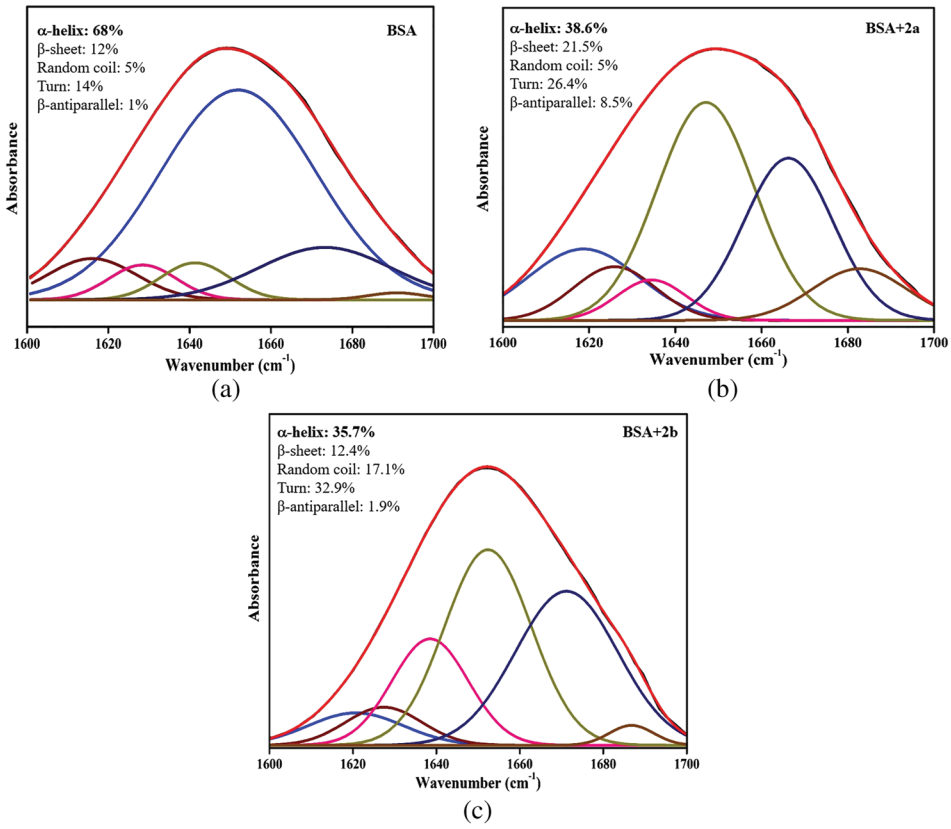

FIGURE 9 Deconvoluted amide I band region of **(a)** BSA (100 μM); **(b)** BSA (100 μM) added with $[V^{IV}O\{(hpdbal)_2\text{-an}\}]$ (50 μM) and **(c)** BSA (100 μM) added with $[V^{IV}O\{(hpdbal)_2\text{-an}\}]$ (100 μM)

subunit and blocking the signaling cascade for the uptake of glucose by the glucose transporter in a type II diabetic patient.

4 | CONCLUSIONS

In this study, novel vanadium (IV) and iron (III) complexes tethered with a O_2N_2 salan ligand were developed and studied for their antidiabetic potential. $[V^{IV}O\{(hpdbal)_2\text{-an}\}]$ was found to excellently induce fluorescent glucose uptake of 95.4% by the insulin resistant cells whose activity was very much higher than the standard drug metformin which is the most commonly prescribed type II antidiabetic drug. $[\{Fe^{III}(OH_2)((hpdbal)_2\text{-an})\}_2\ \mu_2\text{-}SO_4]$ exhibited moderate activity which is almost similar to the metformin activity. Both the compounds showed no significant changes in varying pH media and exhibited optimum pK_a values which suggest their stability in biological pH conditions. The active vanadium complex was found to interact with a carrier protein BSA in an extensive manner through strong interactions which further suggest that the potent drug candidate can be easily transported in serum media through the biological membrane barrier.

As an overall, the authors believe that this work will, in future, pave the road for the design and development of many more potent antidiabetic drug candidates for safe and effectual usage.

ACKNOWLEDGMENTS

Authors are grateful to Science and Engineering Research Board (SERB), India [SB/FT/CS-100/2013] and Department of Science and Technology (DST), India [BT/PR10353/PFN/20/889/2013] for providing the necessary financial help. Authors are also thankful to Nanomission project [SR/NM/NS-20/2014] for providing with EDS characterization facility and Centre for Nano and Material Sciences, Jain University, India for providing with the required infrastructure.

CONFLICT OF INTEREST

There are no conflicts to declare.

ORCID

Amit Kumar https://orcid.org/0000-0001-9760-6233

REFERENCES

[1] (a)*Global report on diabetes*, World Health Organization, Geneva 2016. (b)*IDF Diabetes Atlas 8th Edition 2017 Global fact sheet*, International Diabetes Federation, Belgium **2017**.

[2] A. A. Tahrani, A. H. Barnett, C. J. Bailey, *Nat. Rev. Endocrinol.* **2016**, *12*, 566.

[3] A. J. Krentz, C. J. Bailey, *Drugs* **2005**, *65*, 385.

[4] T. Dujic, K. Zhou, L. A. Donnelly, R. Tavendale, C. N. Palmer, E. R. Pearson, *Diabetes* **2015**, *64*, 1786.
[5] C. J. Bailey, *Clin. Pharmacol. Ther.* **2015**, *98*, 170.
[6] (a)E. O. Billington, A. Grey, M. J. Bolland, *Diabetologia* 2015, *58*, 2238. (b)A. A. Tahrani, A. H. Barnett, C. J. Bailey, *Lancet Diabetes Endocrinol.* **2013**, *1*, 140.
[7] E. Ferrannini, R. A. DeFronzo, *Eur. Heart J.* **2015**, *36*, 2288.
[8] (a)M. Kongot, A. Kumar, *Sci. Rep.* 2018, *55*, 41. (b) T. Mukherjee, J. C. Pessoa, A. Kumar, A. R. Sarkar, *Dalton Trans.* 2013, *42*, 2594. (c)M. R. Maurya, C. Haldar, A. A. Khan, A. Azam, A. Salahuddin, A. Kumar, J. C. Pessoa, *Eur. J. Inorg. Chem.* 2012, *2012*, 2560. (d)T. Mukherjee, J. C. Pessoa, A. Kumar, A. R. Sarkar, *Dalton Trans.* **2012**, *41*, 5260.
[9] J. L. Domingo, M. Gomez, *Food Chem. Toxicol.* **2016**, *95*, 137.
[10] D. Rehder, *Inorg. Chem. Commun.* **2003**, *6*, 604.
[11] S. W. Taylor, B. Kammerer, E. Bayer, *Chem. Rev.* **1997**, *97*, 333.
[12] R. E. Berry, E. M. Armstrong, R. L. Beddoes, D. Collison, S. N. Ertok, M. Helliwell, C. D. Garner, *Angew. Chem. Int. Ed.* **1999**, *38*, 795.
[13] (a)J. M. Winter, B. S. Moore, *J. Biol. Chem.* 2009, *284*, 18577. (b)M. R. Maurya, A. Kumar, J. C. Pessoa, *Coord. Chem. Rev.* **2011**, *255*, 2315.
[14] B. Lyonnet, X. Martz, E. Martin, *Presse Med.* **1899**, *32*, 191.
[15] C. E. Heyliger, A. G. Tahiliani, J. H. McNeill, *Science* **1985**, *227*, 1474.
[16] J. H. McNeill, V. G. Yuen, H. R. Hoveyda, C. Orvig, *J. Med. Chem.* **1992**, *35*, 1489.
[17] K. H. Thompson, C. Orvig, *Met. Ions Biol. Syst.* **2004**, *41*, 221.
[18] K. H. Thompson, J. Lichter, C. LeBel, M. C. Scaife, J. H. McNeill, C. Orvig, *J. Inorg. Biochem.* **2009**, *103*, 554.
[19] D. C. Crans, *J. Inorg. Biochem.* **2000**, *80*, 123.
[20] H. Sakurai, H. Sano, T. Takino, H. Yasui, *J. Inorg. Biochem.* **2000**, *80*, 99.
[21] B. A. Reul, S. S. Amin, J.-P. Buchet, L. N. Ongemba, D. C. Crans, S. M. Brichard, *Br. J. Pharmacol.* **1999**, *126*, 467.
[22] N. Durai, G. Saminathan, *J. Clin. Biochem. Nutr.* **1997**, *22*, 31.
[23] J. W. Morgan, E. Anders, *Proc. Natl. Acad. Sci.* **1980**, *77*, 6973.
[24] A. C. Dlouhy, C. E. Outten, *Met. Ions Life Sci.* **2013**, *12*, 241.
[25] S. J. Lippard, J. M. Berg, *Principles of Bioinorganic Chemistry*, University Science Books, Mill Valley **1994**.
[26] K. P. Maier, H. Kopf, E. W. Neuse, *J. Cancer Res. Clin. Oncol.* **1984**, *108*, 336.
[27] M. Patra, G. Gasser, *Nat. Rev. Chem.* **2017**, *1*, 1.
[28] W. A. Wani, U. Baig, S. Shreaz, R. A. Sheikh, P. F. Iqbal, E. Jameel, A. Ahmad, S. H. Mohd-Setapar, L. T. Hun, *New J. Chem.* **2015**, *40*, 1063.
[29] R. K. Dubey, U. K. Dubey, S. K. Mishra, *J. Coord. Chem.* **2011**, *64*, 2292.
[30] R. Gust, D. Posselt, *Metal salophen complexes for prevention and treatment of cancer*, WO 2008/090081, **2008**.
[31] S. S. Mandal, K. I. Ansari, J. D. Grant, Apoptotic and anti-tumor activities of metallosalens, Us 8198322, **2009**.
[32] R. A. Row, M. M. Jones, *Inorg. Synth.* **1957**, *5*, 113.
[33] (a)M. Kongot, N. Dohare, V. Singh, D. Reddy, N. K. Singhal, R. Patel, A. Kumar, *Eur. J. Pharm. Sci.* 2018, *123*, 335. (b) M. Kongot, N. Dohare, D. S. Reddy, N. Pereira, R. Patel, M. Subramanian, A. Kumar, J. Trace, *Elem. Med. Biol.* **2019**, *51*, 176.
[34] C. Zou, Y. Wang, Z. Shen, *J. Biochem. Biophys. Methods* **2005**, *64*, 207.
[35] (a) N. H. Holyk, *An electron paramagnetic resonance study of model oxovanadium (IV) complexes in aqueous solution; Correlation of magnetic properties with ligand type and metal structure*, MS Thesis submitted to University of New Hampshire, Durham, New Hampshire, 1979. (b)N. D. Chasteen, *Biological Magnetic Resonance*, Plenum Press, New York **1981**.
[36] G. R. Hausen, T. A. Kabanos, A. D. Keramidas, D. Mentzafos, A. Terzis, *Inorg. Chem.* **1992**, *31*, 2587.
[37] E. Garribba, G. Micera, A. Panzanelli, D. Sanna, *Inorg. Chem.* **2003**, *42*, 3981.
[38] (a)M. Kongot, D. Reddy, V. Singh, R. Patel, N. K. Singhal, A. Kumar, *New J. Chem.* 2019, *43*, 10932. (b)M. Joseph, A. Sreekanth, V. Suni, M. R. P. Kurup, *Spectrochim. Acta A Mol. Biomol. Spectrosc.* **2006**, *64*, 637.
[39] (a)H. Fischer, R. Gottschlich, A. Seelig, *J. Membr. Biol.* 1998, *165*, 201. (b)D. T. Manallack, *Perspectives in Med. Chem.* **2007**, *1*, 25.
[40] (a)B. Ojha, G. Das, *J. Phys. Chem. B* 2010, *114*, 3979. (b) M. Kongot, D. Reddy, V. Singh, R. Patel, N. K. Singhal, A. Kumar, *Spectrochim. Acta A Mol. Biomol. Spectrosc.* 2019, *212*, 330. (c)M. Kongot, N. Maurya, N. Dohare, M. Parray, J. Kumar, A. Kumar, R. Patel, *J. Biomol. Struct. Dyn.* **2018**, *36*, 1161.
[41] (a)D. Rehder, *Dalton Trans.* 2013, *42*, 11749. (b)E. Kioseoglou, S. Petanidis, C. Gabriel, A. Salifoglou, *Coord. Chem. Rev.* **2015**, *301*, 87.

SUPPORTING INFORMATION

Additional supporting information may be found online in the Supporting Information section at the end of this article.

How to cite this article: Kongot M, Reddy DS, Singh V, Patel R, Singhal NK, Kumar A. Oxidovanadium (IV) and iron (III) complexes with O_2N_2 donor linkage as plausible antidiabetic candidates: Synthesis, structural characterizations, glucose uptake and model biological media studies. *Appl Organometal Chem*. 2019;e5327. https://doi.org/10.1002/aoc.5327